Mineralogical Diversity in Lake Pavin: Connections with Water Column Chemistry and Biomineralization Processes

Jennyfer Miot, Didier Jézéquel, Karim Benzerara, Laure Cordier, Sara Rivas-Lamelo, Fériel Skouri-Panet, Céline Férard, Mélanie Poinsot, Elodie Duprat

minerals

MDPI

Article

Mineralogical Diversity in Lake Pavin: Connections with Water Column Chemistry and Biomineralization Processes

Jennyfer Miot [1,*], Didier Jézéquel [2], Karim Benzerara [1], Laure Cordier [2], Sara Rivas-Lamelo [1], Fériel Skouri-Panet [1], Céline Férard [1], Mélanie Poinsot [1] and Elodie Duprat [1]

[1] Institut de Minéralogie, Physique des Matériaux et Cosmochimie, Sorbonne Universités, Muséum National d'Histoire Naturelle, CNRS UMR 7590, Université Pierre et Marie Curie, IRD 206, 4 place Jussieu, 75252 Paris cedex 05, France; karim.benzerara@impmc.upmc.fr (K.B.); sara.rivas@impmc.upmc.fr (S.R.-L.); feriel.skouri@impmc.upmc.fr (F.S.-P.); celine.ferard@impmc.upmc.fr (C.F.); melanie.poinsot@impmc.upmc.fr (M.P.); elodie.duprat@impmc.upmc.fr (E.D.)

[2] Institut de Physique du Globe de Paris—Sorbonne Paris Cité—Université Paris Diderot, UMR CNRS 7154, 1 rue Jussieu, 75238 Paris cedex 05, France; jezequel@ipgp.fr (D.J.); cordier@ipgp.fr (L.C.)

* Correspondence: jmiot@mnhn.fr; Tel.: +33-1-4079-4839; Fax: +33-1-4079-3876

Academic Editor: Karen Hudson-Edwards
Received: 29 January 2016; Accepted: 16 March 2016; Published: 23 March 2016

Abstract: As biominerals are good tracers of microbial interactions with the environment, they may provide signatures of microbial evolution and paleoenvironmental conditions. Since modern analogues of past environments help with defining proxies and biosignatures, we explored microbe mineral interactions in the water column of a maar lake, located in France: Lake Pavin. This lake is considered as a potential Precambrian ocean analogue, as it is ferruginous and meromictic, *i.e.*, stratified with a superficial O_2-rich layer (mixolimnion) and a deeper permanently anoxic layer (monimolimnion). We combined bulk chemical analyses of dissolved and particulate matter in combination with electron microscopy analyses of the particulate matter at different depths along the water column. The mineralogy changed along with water chemistry, and most of the minerals were intimately associated with microorganisms. Evolution of the redox conditions with depth leads to the successive precipitation of silica and carbonates, Mn-bearing, Fe-bearing and S-containing phases, with a predominance of phosphates in the monimolimnion. This scheme parallels the currently-assessed changes of microbial diversity with depth. The present results corroborate previous studies that suggested a strong influence of microbial activity on mineralogical diversity through extracellular and intracellular biomineralization. This paper reports detailed data on mineralogical profiles of the water column and encourages extended investigation of these processes.

Keywords: biomineralization; meromictic lake; iron phosphate; magnetite; intracellular carbonate; SEM; TEM; sulfate-reducing bacteria; mercury sulfide

1. Introduction

The major changes of the environmental conditions on the Earth's surface over 4.5 billion years have driven a significant diversification of mineral species [1]. Diverse microbial metabolisms, such as oxygenic photosynthesis or sulfate reduction, have impacted these environmental changes [2,3]. Moreover, microorganisms can directly influence mineral formation via biomineralization [4]. Therefore, linking mineralogical and microbial diversities in modern environments is crucial to understand microbe-mineral interactions in the past, *i.e.*, from the first steps of microbial life onward. Among the modern environments that provide conditions analogous to those supposed to have

dominated on early Earth, meromictic lakes are first choice sites [5]. Indeed, such lakes are permanently stratified with a superficial O_2-rich layer (the mixolimnion, affected by seasonal mixing) and a deeper anoxic layer (the monimolimnion, never intermixed with the upper layer) separated by a zone called the oxycline exhibiting strong O_2 gradients. This setting is very close to the oceanic stratification that may have been widespread before the Great Oxygenation Event (GOE) on the Archean Earth [6,7]. In addition, some meromictic lakes are ferruginous, which is an additional property shared with Archean and Proterozoic oceans [8–11]. Finally, whereas most stratified water bodies (e.g., the Black Sea) are euxinic and, thus, good analogues of the period following the GOE, non-sulfidic meromictic lakes may constitute good analogues of the pre-GOE ocean [5,12].

Iron-cycling bacteria and sulfur-cycling microorganisms have been considered as major players in Precambrian oceans [13–15]. Similarly, modern meromictic lakes studied so far were shown to host a diversity of microorganisms, especially with metabolisms involved in Fe and S biogeochemical cycles. Such metabolisms may contribute to mineral formation through biomineralization processes:

(1) For example, photoferrotrophs have been identified in meromictic Lake Matano (Indonesia) and Lake La Cruz (Spain) [16,17]. Such bacteria are known to promote the formation of Fe-oxyhydroxides, such as goethite [18,19].
(2) Nitrate-dependent Fe(II)-oxidizing bacteria may also be present in the water column of meromictic lakes, as suggested by electron and X-ray microscopy analyses of Lake Pavin samples [20]. This metabolism has been shown to promote Fe-oxyhydroxide and Fe-phosphate precipitation, leading to bacterial cell encrustation [21–23].
(3) Dissimilatory Fe(III)-reducing bacteria (DIRB) have been identified in Lake Pavin [24]. DIRB may be responsible for the formation of green rust (a mixed valence Fe-mineral) in Lake Matano [25–29]. Alternatively, green rust may result from microbial Fe(II) oxidation [30,31].
(4) Finally, multiple sulfur-cycling microorganisms are present in these lakes [17,32]. Chemical and Fe isotope analyses of sedimentary pyrite (FeS_2) suggest that these microbes may contribute to Fe sulfide precipitation in the water column [5,33,34].

All of these biomineralization processes may contribute to a diversity of mineral phases and more or less distinctive biomineralization patterns, *i.e.*, the ways mineral phases are arranged with biological (ultra-)structures. For instance, cells may become encrusted (at their surface and within their cell wall) by Fe-bearing minerals [21,35]. Alternatively, Fe minerals may precipitate at the surface of extracellular organic templates, such as EPS (extracellular polymeric substances) or organic filaments emerging from cells [19,36,37]. Finally, biominerals may form intracellularly [38–41]. The resulting biomineralization patterns may give some clues about the involved microbial diversity and biological processes.

All of these processes have been mostly studied at redox boundaries within sediments. For instance, anaerobic Fe(II)-oxidizing bacteria at sediment redox interfaces contribute actively to the biomineralization of diverse Fe-oxyhydroxides and to Fe and N cycling [42]. Moreover, multiple studies evidenced the presence of sulfur-cycling microorganisms (e.g., sulfate reducing and sulfur oxidizing microbes) at redox boundaries in anoxic sediments [43,44]. In contrast, the diversity of mineral phases and patterns across redox boundaries within the water column of meromictic lakes, as well as their connection with microbial activity remains poorly documented, although such environments offer optimal conditions for sampling and studying neo-formed minerals.

In the present study, we explored the mineralogical diversity and the chemical composition of the water column in the meromictic Lake Pavin (Massif Central, France). This maar lake is ferruginous (total Fe(II) concentrations reaching more than 1 mM) and displays very low free sulfide concentrations [33,45,46]. The redoxcline located at around a 55-m depth constitutes the upper limit of the monimolimnion, which extends down to a 92-m depth. In five successive sampling campaigns, water samples were prepared for chemical and electron microscopy analyses, to get insight into the nature, composition, structure and morphology of the minerals formed in the water column, as a function of geochemical parameters, including major elements' concentrations in the dissolved and

particulate phases, pH and turbidity. Here, we report chemical data from the May 2014 campaign, as well as microscopy observations of samples collected in the five different sampling campaigns that we found to be representative of the mineralogical diversity of the lake over this three-year survey. Whereas the seasonal variations of the chemistry and mineralogy are not explored in the present study, the potential relationships between the formed minerals and the activity of microorganisms is discussed as a basis for future in-depth studies of C, P, Fe and S biogeochemical cycles at this site.

2. Experimental Section

2.1. Geochemistry of Lake Pavin

Samples were collected in the water column from a platform located at the center of Lake Pavin (Massif Central, France) with a Niskin bottle (either 5.6 or 20 L, General Oceanics) during 5 different campaigns (June 2013, November 2013, May 2014, September 2014 and June 2015). A set of geochemical parameters (temperature, dissolved oxygen, conductivity, pH and turbidity) were measured *in situ* during each sampling campaign, using CTD (conductivity-temperature-depth) and a O_2-pH-redox probe (YSI 6600), oxygen optodes (nke SDOT) and a turbidimeter (nke STBD 300). Only the geochemical data from the May 2014 campaign are provided in the present paper. The time variability of these geochemical parameters is briefly discussed.

2.2. Chemical Analyses

For the analysis of dissolved compounds, water samples were filtered on board using syringes and filters with a Luer connection (Whatman, Maidstone, UK, 0.2 µm) and distributed in Falcon® PP tubes (Corning, Mexico City, Mexico) (acidified with Suprapur HNO_3 for ICP-AES analysis). Sulfides were stabilized by precipitation with zinc (+100 µL Zn acetate 0.01 M for a 10-mL sample); this tube was used for both sulfate and sulfide determinations. Sulfide species determined by this method comprise free H_2S and HS^-, as well as metal-bound sulfide nanoparticles (in particular, nanoparticles of FeS, as discussed later [33]). A glass tube (Exetainer Labco, Lampeter, Wales) was filled without air bubbles for alkalinity measurement and a second one for nitrogen species. SPM (suspended particulate matter) was collected by filtration on quartz fiber filters (Whatman, 47 mm diameter; previously grilled, washed and pre-weighted), using a lab-made system suitable to filtrate 4.25 L of water per batch. Contact with air was avoided by N_2 flushing of the filtration system and O_2 concentration monitoring (optode and WTW 3430, Weilheim, Germany) during the entire filtration sequence. Water samples were directly injected from the Niskin bottle in the filtration unit when O_2 concentration in the gas outlet of the unit was less than 1%. After drying and weighing, quartz filters were soaked in 10 mL HNO_3 1 M solution for at least 1 day at room temperature to ensure complete SPM dissolution before ICP-AES analyses (under these conditions, dissolution is supposed to affect the labile and reactive pool of the SPM only; filters totally turned white after treatment, whereas they were colored by particles after filtration).

Anion analyses were performed by ionic chromatography (ICS1100 Thermofisher, Villebon-sur-Yvette, France); concentrations of major and minor elements (Li, Na, K, Mg, Ca, Sr, Ba, Al, B, S, P, Si, Fe, Mn) were measured by ICP-AES (Thermo Scientific iCAP 6200, Villebon-sur-Yvette, France). The concentrations of nitrogen species (NH_4^+/NO_2^-/NO_3^-), DIP (dissolved inorganic phosphorus) (Autoanalyser AxFlow Quaatro, Axflow, Plaisir, France), H_2S (Spectroquant, Merck Millipore, Darmstadt, Germany, methylene blue method) and alkalinity [47] were measured by colorimetry.

2.3. Electron Microscopy

2.3.1. Sample Preparation

For electron microscopy analyses, water from the anoxic depths was collected under N_2 or Ar flux and stored in bottles with an Ar or N_2 headspace, closed with a crimped butyl rubber stopper in order to preserve anoxic conditions.

For SEM analyses, samples were prepared by filtration of a volume of lake water through a polycarbonate GTTP 0.2-µm filter in a Swinnex filter holder, subsequently rinsed with 40 mL of Milli-Q® water (Merck Millipore, Darmstadt, Germany). These filtrations were performed either immediately or a maximum of 3 days after sampling. Filters were mounted on aluminum stubs using double-sided carbon tape and were carbon coated.

For TEM analyses, samples were centrifuged for 10–20 min at 7000 *g*, rinsed three times in Milli-Q® water and deposited on ionized formvar-carbon 200-mesh copper grids. Alternatively, the <200-nm fraction was prepared by filtration through a polycarbonate GTTP 0.2-µm filter, followed by concentration of the particles suspended in the filtrate in an Amicon cell (Merck Millipore) under N_2 flow. Particles were then deposited on a formvar-carbon 200-mesh copper TEM grid before observation.

All air-sensitive samples (collected at the oxycline or in the monimolimnion) were prepared in an anoxic glovebox (<50 ppm O_2) and rinsed with degassed Milli-Q® water.

2.3.2. Scanning Electron Microscopy

SEM observations were performed using a ZEISS Ultra 55 SEM (Zeiss, Marly-le-Roi, France) equipped with a field emission gun (FEG) in secondary electron mode at 3 kV and a working distance (WD) of 2.5 mm using the in-lens detector. Alternatively, samples were imaged at 10 kV and a WD of 7.5 mm using the SE2 detector. Energy dispersive X-ray spectrometry (EDXS) analyses were conducted at 15 kV and a WD of 7.5 mm after calibration with reference copper.

2.3.3. Transmission Electron Microscopy

TEM analyses were performed using a FEG JEOL2100F microscope (JEOL, Croissy, France) operating at 200 kV. Selected area diffraction (SAED) patterns were obtained on areas of interest to characterize amorphous *vs.* (nano)crystalline mineral phases. Scanning transmission electron microscopy (STEM) analyses were conducted in high angle annular dark field (HAADF) mode and combined with EDXS mapping.

3. Results and Discussion

The geochemical profiles of Lake Pavin in May 2014 are typical of a meromictic lake (Figure 1) and of the geochemistry typically observed in this lake [46]. Spring 2014 followed a winter without complete mixing of the mixolimnion. Consistent with previous descriptions [5,20,45,46,48,49], it is characterized by a sharp turbidity peak at around a 55-m depth, just below the O_2 transition zone between the oxic (mixolimnion) and anoxic (monimolimnion) layers. The pH of the lake was higher in the mixolimnion (up to pH 8) and stabilized around 6.3 in the monimolimnion. As suggested by the turbidity and conductivity profiles, concentrations in dissolved and particulate species strongly changed along the water column and were related to the precipitation of various mineral phases with depth, as described in the following sections.

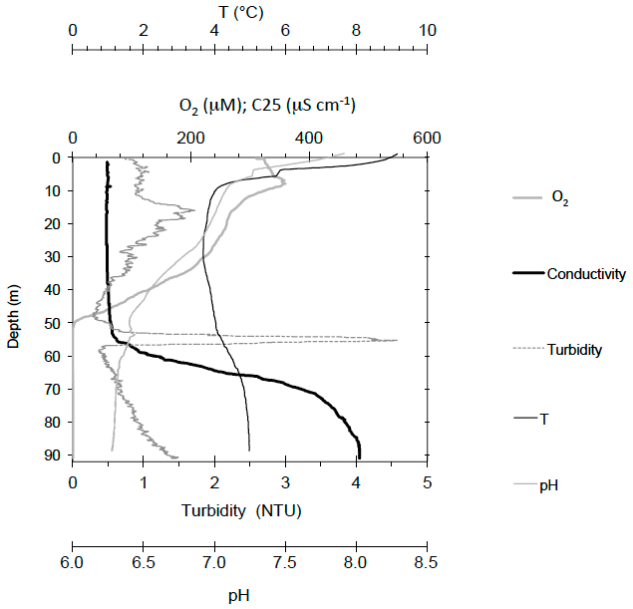

Figure 1. Geochemical profiles in the water column of Lake Pavin. Conductivity (C25), temperature (T), pH, dissolved oxygen concentration (O_2) and turbidity profiles (May 2014).

3.1. Mineral Phases in the Superficial Zone of the Lake (0–30-m Depth)

A turbidity peak was observed in the mixolimnion at around a 17-m depth (Figure 1). This peak has been shown to exhibit a variable intensity depending on the season and year: it is sharper in spring and early summer and has been shown to be related to algal blooms [50,51]. Diatom frustules were predominant at these depths for the five sampling campaigns and contributed to massive precipitation of silica in the lake. Consistent with a previous quantification [45], we observed qualitatively by SEM that these silica biominerals were by far the most abundant mineral phases in the water column over this three-year survey.

At these depths (0–30 m), mineralogical diversity was very limited. A few detrital particles, with various sizes, were observed, usually exhibiting an iron aluminosilicate composition. This is in accordance with previous X-ray absorption spectroscopy analyses that identified phyllosilicates as the main Fe-bearing phases in the monimolimnion [20].

In this oxic part of the lake, multiple bacteria hosted intracellular granules rich in phosphorus with Ca, K and Mg, interpreted as polyphosphate globules (Figure 2a,b). The abundance of polyphosphates has been noted by [20] and suggests the existence of active P sequestration processes mediated by diverse bacteria. Interestingly, for two different sampling campaigns (June 2013, May 2015), we also observed at a 20-m depth a few cells with intracellular inclusions rich in carbon and calcium. These inclusions displayed an amorphous SAED pattern and were therefore identified as amorphous calcium carbonate (Figure 2c,d). A wide diversity of early-branching cyanobacteria in various habitats have been shown to promote intracellular precipitation of amorphous calcium carbonate [39,40]. Although further characterization of these microorganisms in Lake Pavin will be needed in order to check their phylogenetic affiliation, we can speculate that they are cyanobacteria based on this specific biomineralization pattern and their occurrence in the photic zone. In any case, this adds to the diversity of environments hosting such microorganisms forming intracellular carbonates [52]. Given the supposed geochemical similarities between Lake Pavin and Precambrian environments [5,12], these observations suggest that such a biomineralization process may have occurred in past environments, as well.

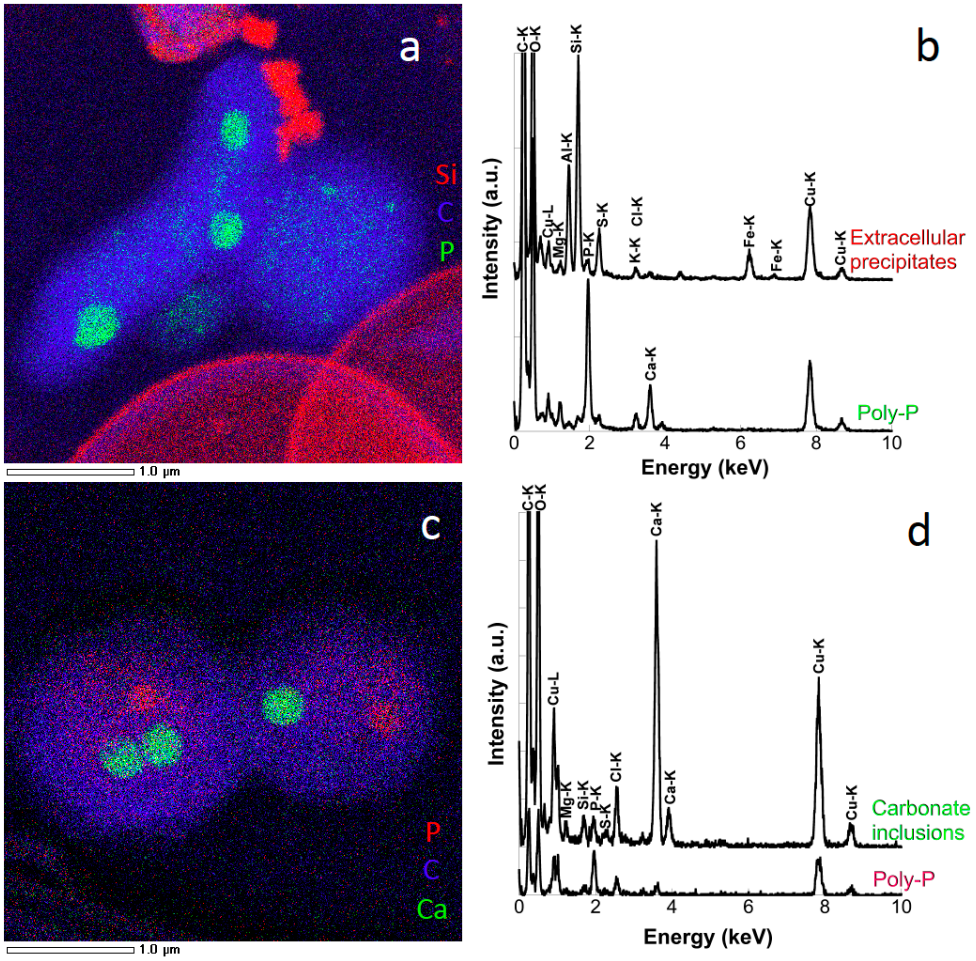

Figure 2. Intracellular carbonate and phosphate inclusions in bacteria collected at 17-m (**a**,**b**) and 20-m (**c**,**d**) depths respectively. (a) STEM-EDXS map at a 17-m depth (June 2015) with poly-phosphate granules in green and silica in red and (c) STEM EDXS map at a 20-m depth (May 2015) with carbonate inclusions in green and poly-P granules in red; (b,d) corresponding EDXS spectra.

3.2. Transition from Mn- to Fe-Mineral Formation (50–60-m Depth)

Successive strong enrichments in Mn (centered at a 49-m depth in May 2014) and Fe (centered at a 55-m depth in May 2014, *i.e.*, approximately at the maximum of turbidity) were observed in the particulate matter by bulk analyses (Figure 3f). Whereas O_2 was still present at the depth of maximum particulate Mn concentration, the particulate Fe concentration maximum was located in the anoxic part of the lake. Consistently, we observed by SEM a shift in the chemical composition of minerals formed at these depths from Mn-bearing phases to Fe-bearing phases (Figure 3). Around a 49-m depth, numerous Mn-bearing phases were observed. All of them were more or less enriched in phosphorus, suggesting they consist of manganese phosphates or potentially manganese oxides with significant amounts of adsorbed phosphate (Figure 3a). These phases appeared as agglomerates of nm-scale marbles (100–300 nm in diameter) or exhibited a specific star-like morphology (Figure 3e). Most of the Mn oxidation in aquatic environments is attributed to the activity of Mn-oxidizing bacteria, because abiotic Mn oxidation is kinetically limited at circumneutral pH, and Mn-oxidizing bacteria are widespread in aquatic environments, especially at oxic-anoxic interfaces, and contribute to the formation of Mn-oxides [53]. They are widely distributed across the bacterial phylogenetic tree, and various processes of Mn biomineralization have been described, involving either enzymatic processes [54,55] or the export of reactive oxygen species [56], in any case leading to the extracellular formation of Mn-oxides. Specific morphologies of Mn-oxides have been described that are similar to

the present observations [57]. Precipitation of Mn(II)-phosphate in cultures of *Shewanella putrefaciens* has been reported, as well [58]. Noteworthy, Mn-bearing phases have been characterized by EXAFS at the oxic-anoxic boundary of the eutrophic Lake Sempach (Switzerland) [59]. They consisted of H^+-birnessite (MnO_2) in the oxic layer that was reduced to (Ca, Mn)CO_3 and (Fe, Mn)$_3(PO_4)_2 \cdot 8H_2O$ particles in the anoxic layer (in the sediment). In contrast, rapid Mn reduction in the water column of the meromictic and ferruginous (but phosphate-poor) Lake Matano precluded the deposition of Mn-bearing minerals to the sediments [60]. It would be of interest to investigate more deeply the speciation of Mn in the Mn-oxides and phosphates formed in the Lake Pavin water column, as well as their fate in the sediment, and to explore the microbial diversity potentially involved in the Mn biogeochemical cycle in this lake.

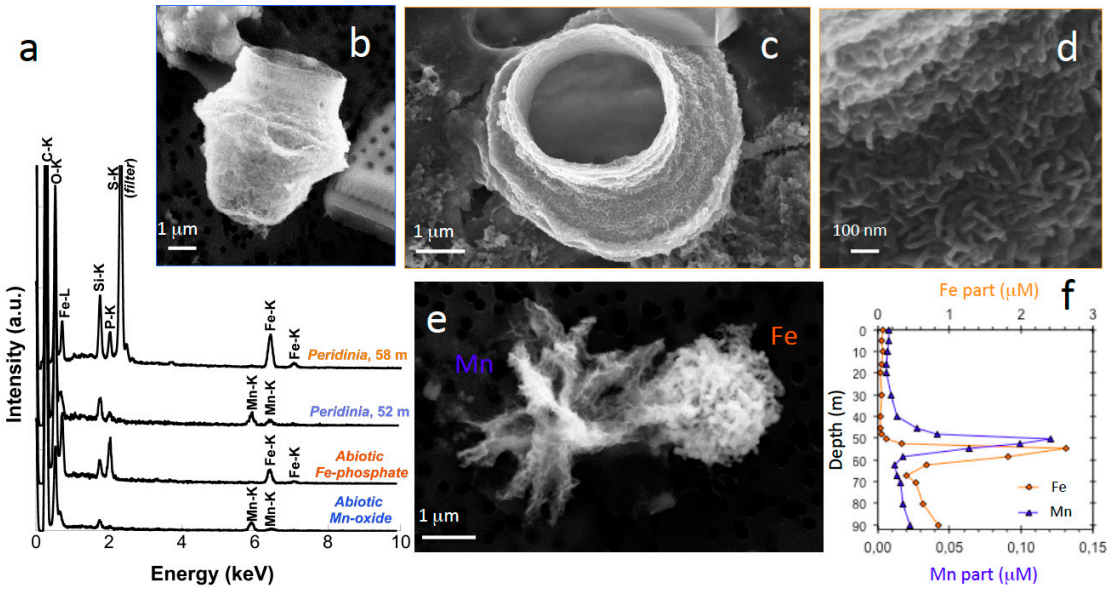

Figure 3. Transition from Mn to Fe mineral compositions with depth. (**a**) EDXS analyses of the corresponding SEM images; (**b**–**d**) SEM images of *Peridinia* frustules covered with Mn (52-m depth, May 2014; (**b**)) or Fe (58-m depth, June 2013; (**c**,**d**)) phosphate; (**e**) SEM image of extracellular minerals precipitated at 52 m (May 2014); (**f**) profiles of Fe and Mn concentrations in the particulate matter of Lake Pavin (May 2014).

Just above the turbidity peak (at around a 52-m depth in May 2014), Mn-bearing phases sometimes coexisted with Fe- and P-rich phases (Figure 3e). A few mixed phosphates composed of both Fe and Mn were observed, as well. This transition from Mn-phosphates to Fe-phosphates was remarkably recorded by dinoflagellates of the *Peridinium* genus (Figure 3a–d). These protists were only observed in some campaigns (June 2013, May 2014) and at specific depths (typically between a 50- and a 60-m depth), which is in accordance with the description of spring dinoflagellate blooms, including *Peridinium willei*, in this lake [61]. Whereas *Peridinia* theca were encrusted by Mn phosphates at a 52-m depth (Figure 3a,b), the encrustation composition evolved towards mixed Fe and Mn-phosphate just below this depth and, finally, Fe-phosphate alone below a 58-m depth (Figure 3a,c,d). Fe-phosphates covering the entire surface of these protists exhibited a very specific "noodle-like" texture, with ~100-nm long sticks (Figure 3d). Similar textures were also observed at the surface of micrometer-scale ball-like objects, systematically exhibiting a depression at one pole, but that we were not able to identify further (Figure 4b). As the chemical composition of these minerals followed the evolution of the chemical composition of the water column, we suggest that such textures may arise from passive mineral deposition at the surface of organic structures, *i.e.*, they would be the products of passive biomineralization [4,62].

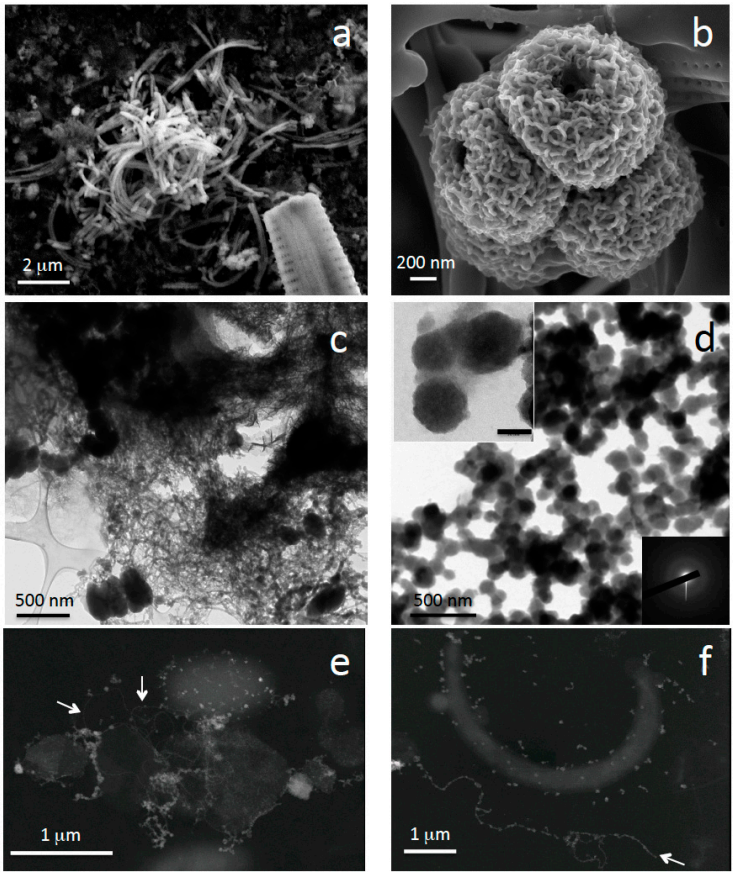

Figure 4. Morphological diversity of Fe phosphates collected at different depths (58 m ((**a**) May 2014; (**b**) June 2013); 56 m ((**c**) November 2013); 67 m ((**d**) May 2014)). SEM images (**a**,**b**) and TEM images (**c**,**d**), with insets showing details of the morphology (upper left, scale bar 50 nm) and SAED pattern of the nanoparticles (lower right); (**e**,**f**) STEM-high angle annular dark field (HAADF) images of bacteria associated with nanoparticles and partly mineralized filamentous structures (60-m depth, June 2015). Arrows point to organic filaments.

3.3. Fe Biomineralization across and below the Oxycline

At and below the turbidity peak (located at a 55-m depth in May 2014), Fe-phosphates are a major phase [20,45,46]. This is consistent with the co-variation of P and Fe concentrations in the particulate matter (Figure 5b). Fe phosphates exhibited a wide diversity of morphologies: a few µm-long curved filaments (Figure 4a), a few nm-long tangled filaments (Figure 4c), 40–50-nm large spherical particles (Figure 4d). In addition, iron phosphate nanoparticles were observed at the surface of microbial cells, whereas some cells exhibited intracellular inclusions of polyphosphate (Figure 5a,c–d), which is consistent with previous reports [20]. The quantitative role of this microbial P storage in the biogeochemical cycles of P and Fe in Lake Pavin remains to be investigated. Moreover, Fe-phosphates precipitated within the water column of Lake Pavin have been previously shown to exhibit a mixed Fe redox state (Fe(II)-Fe(III)-phosphates) [20], which is similar to Fe-phosphates described in the eutrophic stratified Lake Bret (Switzerland) [63,64]. This is also in accordance with experimental oxidation of Fe(II) in solutions enriched in phosphate at neutral pH leading to the precipitation of amorphous Fe(III)-phosphate, more or less enriched in Ca [65]. This oxidation process and the nature of the formed precipitates were recently shown to be influenced by the initial Fe/P ratio [66].

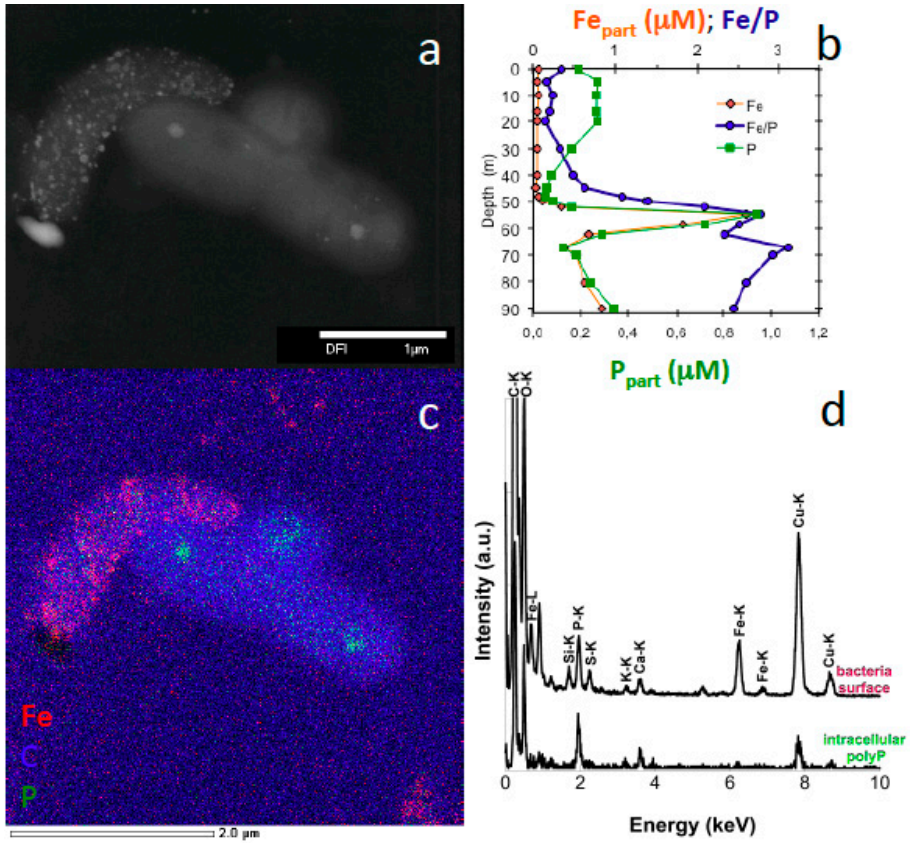

Figure 5. Coexistence of Fe phosphate associated with bacterial surfaces (**red**) and intracellular polyphosphates (**green**) at a 60-m depth (June 2015). (**a**) STEM-HAADF image; (**b**) profiles of P, Fe concentrations and bulk Fe/P atomic ratio in the particulate matter of the lake (May 2014); (**c**) EDXS composite elemental map and (**d**) corresponding EDXS spectra.

In addition, a diversity of Fe-bearing minerals typically formed by biomineralization was observed at and below the oxycline (Figures 6 and 7).

TEM observations of samples collected in June 2015 revealed the presence of magnetotactic bacteria at the oxycline (52.4-m depth) [67] (Figure 6). The redox transition zone is prone to magnetotactic bacteria occurrence, as they are usually observed at the oxycline of marine and lacustrine sediments [68]. These intracellular magnetites contrast with extracellular amorphous Fe-phosphates, and this can be explained as the result of controlled biomineralization providing local intracellular chemical micro-environments very different from those prevailing in the water column.

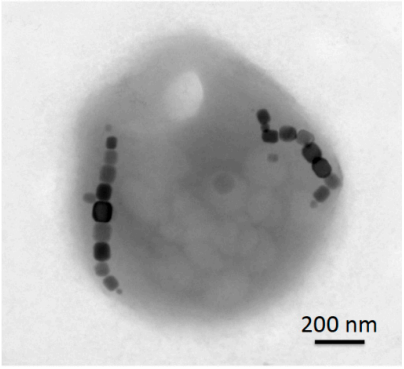

Figure 6. Magnetotactic bacteria at the redoxcline (52.4-m depth) observed by TEM (June 2015).

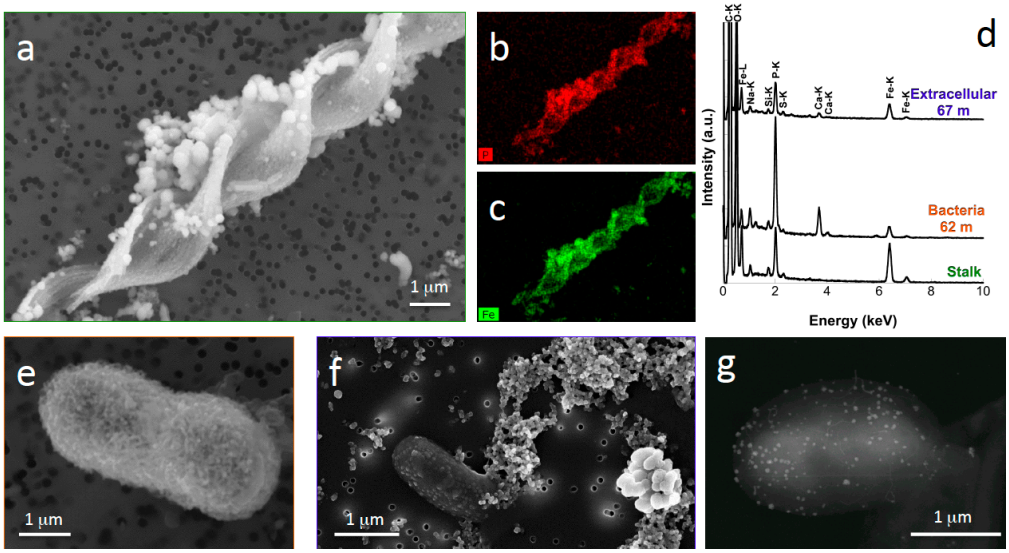

Figure 7. Diversity of Fe biomineralization patterns: (**a**–**c**) *Gallionella*-like stalk biomineralized with Fe-phosphate ((**a**) SEM image; (**b**,**c**) corresponding P and Fe EDXS elemental maps, September 2014); (**d**) EDXS analyses of the stalk (green, (**a**)); bacteria shown in (**e**) (orange) and extracellular precipitates shown in (**f**) (blue); (**e**) SEM image of a microbial cell encrusted with Fe-phosphate (62-m depth, September 2014); (**f**) SEM image of a microbial cell only partially covered by Fe-phosphate and surrounded by numerous extracellular Fe phosphate nanoparticles (67-m depth, September 2014); (**g**) STEM-HAADF image of a microbial cell associated with Fe-phosphate nanoparticles at its surface (80-m depth, June 2015).

In addition, we observed at a 60–62-m depth stalks indicative of extracellular Fe biomineralization promoted by bacteria of the *Gallionella* genus (Figure 7a–d). This is consistent with previous reports of 16S rRNA sequences closely related to *Gallionella ferruginea* in Lake Pavin at a 60-m depth [69]. Such micro-aerophilic species occupy very narrow niches at redox boundaries exhibiting opposite gradients of dissolved Fe(II) and O_2 [70,71]. At the depths where we found these biominerals, O_2 concentration ranged from 0–2 µM, which falls within the tolerance range reported for these microorganisms (<10 µM dissolved O_2) [70]. A diversity of microaerophilic iron(II)-oxidizing bacteria have been shown to produce extracellular organic polymers in the form of tubes or stalks that template iron(III)-bearing mineral precipitation [36,72–75]. Whereas all previously-described *Gallionella* stalks were composed of Fe(III)-oxyhydroxides, such as ferrihydrite, goethite [72,76] or lepidocrocite [36] in association with organic matter, here, they consisted of Fe phosphates (most probably associated with organics) (Figure 7d). This suggests a strong control of the chemical composition of the solution over the composition of these biominerals, whereas organics would act as preferential nucleation sites for the deposition of these phases [33,76]. Whereas Fe phosphates in the mixolimnion of Lake Pavin have been shown to exhibit a mixed Fe redox state [20], it would be of interest to investigate the local Fe redox state of these stalks. Indeed, as they are produced upon microbial Fe(II) oxidation, they may exhibit a Fe redox state different from that of surrounding Fe phosphates. Noteworthy, no cells could be observed in association with these stalks. This is consistent with the scenario of cells extruding their stalks as long as biomineralization proceeds [73]. In addition, such stalks were only observed during some campaigns (September 2014, May 2015), suggesting that they are dominant only in some specific periods of the year or distributed along very narrow niches, which we potentially missed in some field collection campaigns.

Fe-phosphates were also observed in the form of µm-scale bacterial-like structures (Figure 7e) at a 62-m depth. These observations are consistent with previous descriptions of Fe-biomineralized bacteria in this lake based on TEM and STXM analyses at the C K-edge and Fe $L_{2,3}$-edges [20].

Such features are reminiscent of biomineralization patterns observed in laboratory cultures of nitrate-reducing Fe(II)-oxidizing bacteria encrusted with Fe-phosphates [21]. Noteworthy, bulk chemical analyses revealed a consumption of nitrate concomitant with the precipitation of Fe-phosphate at around a 52-m depth (Figure 8; May 2014). Nitrate is thus a good candidate for Fe(II) oxidation at this anoxic depth. In addition, we obtained from these depths some bacterial enrichments promoting Fe-phosphate precipitation under anoxic conditions in the presence of acetate and nitrate as sole electron acceptor (data not shown). Further characterization of these enrichments is in progress. Whereas such a metabolism has been described in several lake sediments [77], it has never been reported in a lake water column. Our preliminary results suggest that microbial nitrate-dependent Fe(II) oxidation may take part in the process of iron biomineralization in this anoxic part of the lake. Further investigations would be necessary to confirm and quantify their role in the Fe cycle of Lake Pavin.

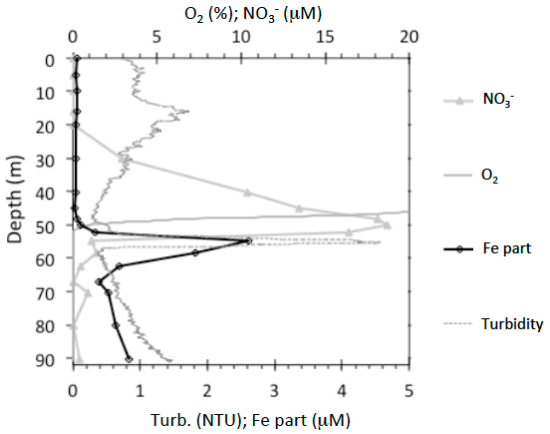

Figure 8. Chemical profiles of dissolved O_2 concentration, nitrate concentration, bulk Fe concentration in the particulate matter and turbidity in Lake Pavin (May 2014).

3.4. Microorganisms: Mineral Interactions down to the Deep Monimolimnion (60–90-m Depth)

With increasing depth, the bacteria we observed were less mineralized and usually associated with nanoparticles of Fe-phosphate (3–5 nm in diameter) at their surface (Figure 7f,g). Concomitantly, extracellular spherical 100–200-nm large amorphous Fe-phosphate particles were dominant, as observed by SEM, TEM, SAED and STEM on non-filtered samples and <200-nm fractions (Figure 4d). It has been shown previously using TEM-EDXS that the Fe/P atomic ratio of Fe phosphates decreased with depth, towards the ratio expected for vivianite ($Fe_3(PO_4)_2 \cdot 8H_2O$; Fe/P = 1.5) [20]. In accordance, experimental Fe(II) oxidation at neutral pH from a solution with an initial Fe/P ratio < 2 led to the formation of amorphous Ca-containing Fe(III)-phosphate with a Fe/P up to 1.4 [66]. Here, bulk Fe/P in the particulate matter in May 2014 decreased down to 2.4 close to the bottom of the lake (Figure 5b), which is lower than the previously-reported values and, thus, different from the Fe/P of vivianite. This may be explained by a large proportion of Fe-phosphate nanoparticles being lost upon filtration through quartz filters.

Some of these particles were associated with 10–20 µm-long organic filaments emerging from and "connecting" bacteria (arrows in Figure 4e,f). These filaments could be either pili or nanowires, as described in some Fe(III)-reducing bacteria [78]. Although facultative (e.g., fermentative *Pseudomonas* and *Clostridium* sp.) Fe(III)-reducers have been previously retrieved from Lake Pavin enrichments [24,79], obligate Fe(III)-reducing bacteria, such as *Geobacter* sp. (some species being known to form electrically-conductive nanowires under some conditions), were not detected. Alternatively, these filaments could also result from the collapse of extracellular organic polymers during sample preparation [80,81]. Indeed, previous STXM analyses at the C K-edge of samples collected in Lake

Pavin at similar depths revealed the presence of extracellular polymeric substances surrounding bacteria and nucleating Fe phosphates [20]. The exact nature and potential function of these organic structures thus remain to be elucidated.

At an ~62-m depth, bulk chemical measurements indicated an enrichment in sulfur species, *i.e.*, free H_2S/HS^- and colloidal FeS (according to the method of determination: reaction with zinc acetate followed by methylene blue dosage), which was shown to be dominant in the monimolimnion [33]. This is correlated with a drop in dissolved sulfate concentration (Figure 9a). Although not measured in May 2014, previous campaign measurements indicated that the minimum in the redox potential occurred close to this depth (e.g., 60 m in September 2014 and 60.7 m in May 2015). This is consistent with previous reports of the variations in concentrations of S compounds in the water column of this lake [33,34,49]. At this depth, several bacteria with intracellular inclusions measuring 500 nm–1 µm in diameter exclusively composed of S were observed in September 2014 (Figure 9c,d,f). They are interpreted as sulfur oxidizing bacteria hosting intracellular accumulations of elemental sulfur. Some bacteria oxidizing reduced sulfur compounds (e.g., H_2S) indeed often store sulfur transiently in the form of intracellular (membrane-bound) or extracellular globules of elemental sulfur during the oxidation of thiosulfate or sulfide [82]. Accordingly, a diversity of sulfur oxidizing prokaryotes has been identified based on aprA (a functional marker) and 16S rRNA gene-based analyses at this depth in Lake Pavin [32]. They include purple sulfur bacteria members of the *Chromatiaceae* family (closely related to a *Thiodictyon* sp. clone) and potential nitrate-reducing sulfide oxidizing bacteria (NRSOB). The presence of anoxygenic photosynthesizers, such as *Chromatiaceae*, is consistent with the amount of photosynthetically-active radiation (measured in the 400–700-nm range) at these depths in September–October [20,83]. Alternatively or in addition, chemolithoautotrophic sulfur oxidizers, such as NRSOB, can oxidize reduced sulfur compounds without any need for light [84]. The presence of NRSOB would be consistent with geochemical parameters in the monimolimnion, *i.e.*, nitrate and free sulfide profiles (Figure 8). Such sulfur oxidizing bacteria have been shown to convert hydrogen sulfide to elemental sulfur [85] and are key players of the sulfur cycle in sulfidic habitats, especially at oxic-anoxic boundaries [86,87]. In addition, we observed several occurrences of minerals composed of barium and sulfur in the monimolimnion (Figure 9e,f). These phases could consist either of barite ($BaSO_4$) or barium sulfides (e.g., BaS). On the one hand, the formation of barite here may connect with the activity of sulfur-oxidizing bacteria [88–90]. On the other hand, it has been proposed that sulfate-reducing bacteria may contribute to the precipitation of barium sulfides [91].

Sulfate-reducing bacteria and archaea taking part in the reductive part of the sulfur cycle have been identified in the monimolimnion of Lake Pavin [32]. Their activity may be responsible for the increase in H_2S concentration below 60 m (Figure 9a). Electrochemical analyses showed that iron sulfide in the form of colloidal FeS occurs in the anoxic part of Lake Pavin, in accordance with thermodynamics predicting the precipitation of mackinawite (and greigite in the upper part of this anoxic layer) [33]. However, our electron microscopy analyses did not evidence any iron sulfide precipitate in the water column, even in the <200-nm fraction and despite multiple samplings (various seasons, years) at multiple depths. This would suggest that either the density of FeS particles in the water column was very low and dominated by colloidal particles and/or that these phases were very reactive and were not preserved during sample preparation, even when processed under anoxic conditions from sampling until complete drying. In contrast, we observed numerous microbial cells covered with Fe-phosphate nanoparticles in all campaigns. In addition, nanoparticles (3–10 nm in diameter) composed of Hg and S were observed by TEM in samples collected in June 2015 (Figure 9b,f). Given their very small size, these nanoparticles, if present in the previous campaigns, may have been overlooked by SEM observations. Based on EDXS analyses, these nanoparticles exhibited an Hg/S atomic ratio close to one, suggesting they consisted of HgS. A diversity of bacteria from various contaminated sites has been shown to sorb mercury at their surface and within extracellular polymeric substances in the form of nanometric spherical precipitates comparable to our observations [92]. In addition, sulfate-reducing bacteria may contribute to HgS precipitation through sulfide production [93]. At the

same time, we cannot exclude that Fe may have been sometimes associated with these precipitates, wherein Hg would be adsorbed onto FeS nanoparticles, as shown by [93]. Sulfate-reducing bacteria are major contributors to the formation of methyl mercury, a neurotoxin that accumulates in the food web. The methylation potential of Hg depends on microbial activity and Hg speciation [94]. For instance, the methylation rate has been shown to decrease with increasing mercuric sulfide aging (from dissolved Hg to nanoparticulate and microcrystalline HgS) [95]. In addition, the association with organic matter would also influence this methylation rate [96]. In the present case, nanoparticulate HgS in the zone hosting sulfate-reducing bacteria may be favorable to the production of methyl mercury. Noteworthy, high concentrations of surface active substances (estimated by their adsorption properties at an Hg electrode) and natural organic matter have been previously reported in the deep monimolimnion [33], which could influence the production of methyl mercury. Elucidating the identity of the microorganisms associated with these HgS nanoparticles and analyzing more extensively sulfur and mercuric species, as well as their potential interactions with natural organic matter in Lake Pavin will provide better insights into the connections between mercury and sulfur cycles in this lake.

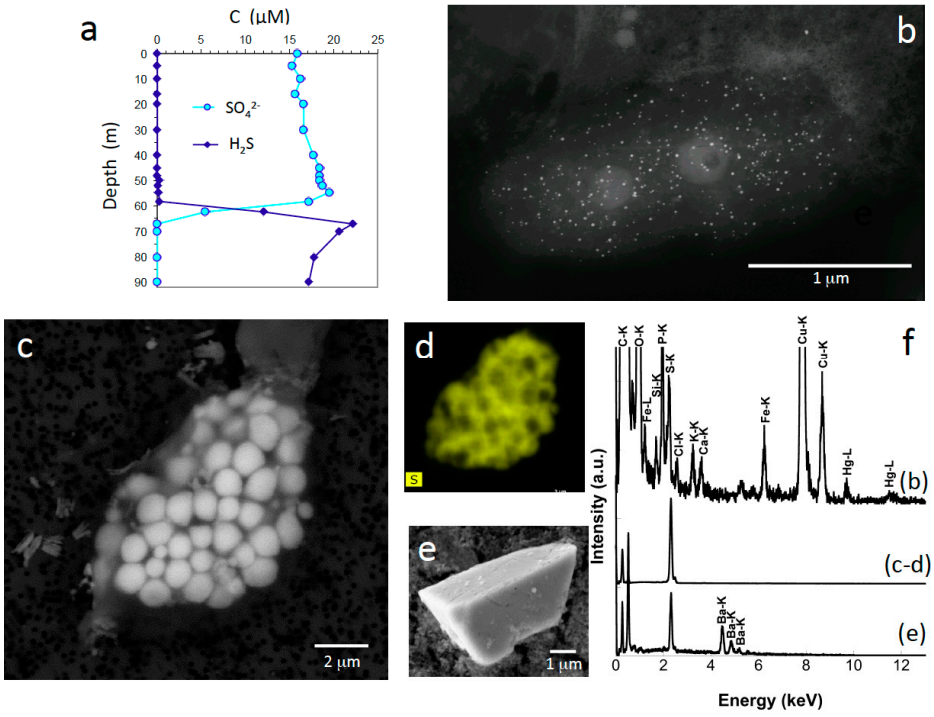

Figure 9. Sulfur speciation in Lake Pavin and potential connections with microbial activity. (**a**) Sulfate and H_2S profiles in the water column of Lake Pavin (May 2014); (**b**) STEM-HAADF image of a microbial cell covered with Fe-phosphate and Hg-bearing nanoparticles (52.4-m depth, June 2015); (**c**) SEM image of a microbial cell (62-m depth) with numerous elemental sulfur inclusions (September 2014) and (**d**) corresponding SEM-EDXS elemental map; (**e**) SEM image of a barium- and sulfur-containing particle (May 2014); (**f**) EDXS analyses of the structures displayed in (**b**–**e**).

4. Conclusions

Lake Pavin shows a remarkable diversity of mineral phases (Table 1). Both abiotic and microbial processes control this mineralogical diversity. The evolution of the redox conditions with depth leads to the successive precipitation of silica and carbonates, Mn-bearing, Fe-bearing and S-containing phases, with a predominance of phosphates in the monimolimnion. This scheme parallels the changes of microbial diversity with depth as currently assessed in the lake water column. The present results corroborate and extend much further previous studies that suggested a strong influence of microbial activity on mineralogical diversity through extracellular and intracellular biomineralization [20,67] and

provide bases for exploring more deeply these processes. Lake Pavin thus appears as a real cornucopia for geomicrobiologists. For instance, it would be of interest to study more extensively the link between cyanobacterial diversity and carbonate precipitation, or to quantify microbial contribution to the phosphorus cycle, or to clarify the diversity and role of Fe(II)-oxidizing and Fe(III)-reducing bacteria in the Fe cycle, or to understand the connections between microbial sulfur cycling and sulfide formation down to the sediment, as well as the connections between S and Fe cycles, including microbial contributions. Moreover, it will be crucial to elucidate the fate of all of these mineral-organics-microbe assemblies upon sedimentation and early diagenesis. Fe isotope analyses of sedimentary pyrites suggested that these minerals record the δ^{56}Fe signature of Fe-phases formed at the oxycline, *i.e.*, within the water column [5]. Evaluating the fate of Fe-minerals formed in the water column upon sedimentation and diagenesis (*in situ*, or through experimental fossilization experiments [97]) would provide additional clues to understand the biogeochemistry of this potential Precambrian ocean analogue and help define proxies to be used for the reconstruction of paleoenvironments.

Table 1. Diversity, depth occurrence and properties of the minerals observed in the Lake Pavin water column.

Minerals	Proposed Chemical Formula	Association with Microorganisms	Morphologies	Approximate Depth Range of Occurrence
Silica	SiO_2	Diatoms	Frustules	All depths, with higher concentrations in the mixolimnion
Phyllosilicate	-	-	-	All depths
Polyphosphate	$H_{(n+2-2x-2y-z)}K_zMg_yCa_xP_nO_{(3n+1)}$	Bacteria	Intracellular globules	All depths, with variations in amplitude depending on depth
Amorphous Ca-carbonate	$CaCO_3$	(Cyano)bacteria	Intracellular globules	20 m
Mn-oxide	MnO_2	-	Star-like and 100–300-nm marbles	52 m
Mn-phosphate	-	-	Star-like and 100–300-nm marbles	52 m
Mn-Fe-phosphate	-	-	Star-like and 100–300-nm marbles	55 m
Mn-phosphate	-	*Peridinia*	Noodle like	52 m
Mn-Fe-phosphate	-	*Peridinia*	Noodle like	55 m
Fe-phosphate	-	*Peridinia*	Noodle like	58 m
Fe-phosphate	-	-	A few micrometer-long filaments, a few nm-long tangled filaments, 40–50-nm large spherical particles	Around the oxycline
Fe-phosphate	-	Bacteria (Fe(II)oxidizing nitrate-reducing bacteria?)	Cell surface encrustation	60–80 m
Fe-phosphate	-	*Gallionella ferruginea*?	Stalks	60–62 m
Fe-phosphate	-	Microbes	Cell surface-associated nanoparticles (3–5 nm)	60–80 m
Fe-phosphate	-	-	100–200-nm large particles	60–90 m
Magnetite	Fe_3O_4	Bacteria	Intracellular chains	Around the oxycline
Sulfur	$S^{(\circ)}$	Sulfur-oxidizing bacteria	Intracellular globules	62 m
Barium and sulfate bearing minerals	BaS or $BaSO_4$	-	Plurimicrometric	67–90 m
Mercuric sulfide	HgS	Sulfate-reducing bacteria?	Nanoparticles (3–10 nm in diameter)	52–80 m

Acknowledgments: We thank Olivier N'Guyen for his valuable contribution to the May 2014 sampling campaign. This work was supported by a PEPS-CNRS grant (program EXOMOD) to Jennyfer Miot, a CNRS grant (program EC2CO) to Elodie Duprat, the SRB project, Grant ANR-14-CE33-0003-01, of the French Agence Nationale de la Recherche (ANR) to Jennyfer Miot and the ERC CALCYAN grant (FP7/2007-2013 Grant Agreement No. 307110) from the European Research Council to Karim Benzerara. The SEM facility of the IMPMC is supported by Région Ile de France Grant SESAME 2006 N°I-07-593/R, INSU/CNRS, UPMC-Paris 6, and by the Agence Nationale de la Recherche (ANR Grant No. ANR-07-BLAN-0124-01). We thank Imene Esteve for her expert support of the SEM at IMPMC. The TEM facility at IMPMC is supported by Région Ile de France Grant SESAME 2000 E 1435. We thank Jean-Michel Guigner for his expert support of the TEM at IMPMC. Part of this work was supported by the IPGP multidisciplinary program PARI and by Région Ile-de-France SESAME Grant No. 12015908. This work was supported by French state funds managed by the ANR within the Investissements d'Avenir program under Reference ANR-11-IDEX-0004-02 and, more specifically, within the framework of the Cluster of Excellence MATISSE led by Sorbonne Universités.

Author Contributions: All authors contributed to sampling. Didier Jézéquel and Laure Cordier performed some of the chemical analyses. Didier Jézéquel performed *in situ* analyses. Jennyfer Miot, Karim Benzerara, Céline Férard, Mélanie Poinsot, Fériel Skouri-Panet and Sara Rivas-Lamelo prepared the samples for microscopy. Jennyfer Miot and Karim Benzerara performed SEM and TEM analyses. All authors contributed to manuscript writing.

Conflicts of Interest: The authors declare no conflict of interest.

References

1. Hazen, R.M.; Papineau, D.; Bleeker, W.; Downs, R.T.; Ferry, J.M.; McCoy, T.J.; Sverjensky, D.A.; Yang, H. Mineral evolution. *Am. Mineral.* **2008**, *93*, 1693–1720. [CrossRef]
2. Ehrlich, H. Geomicrobiology: Its significance for geology. *Earth Sci. Rev.* **1998**, *45*, 45–60. [CrossRef]
3. Nealson, K.H.; Stahl, D.A. Microorganisms and biogeochemical cycles: What can we learn from layered microbial communities? In *Geomicrobiology: Interactions between Microbes and Minerals*; Banfield, J.F., Nealson, K.H., Eds.; Mineralogical Society of America: Chantilly, VA, USA, 1997; Volume 35, pp. 5–34.
4. Benzerara, K.; Miot, J.; Morin, G.; Ona-Nguema, G.; Skouri-Panet, F.; Férard, C. Significance, mechanisms and environmental implications of microbial biomineralization. *C. R. Geosci.* **2011**, *343*, 160–167. [CrossRef]
5. Busigny, V.; Planavsky, N.J.; Jézéquel, D.; Crowe, S.; Louvat, P.; Moureau, J.; Viollier, E.; Lyons, T.W. Iron isotopes in an Archean ocean analogue. *Geochim. Cosmochim. Acta* **2014**, *133*, 443–462. [CrossRef]
6. Crowe, S.A.; Døssing, L.N.; Beukes, N.J.; Bau, M.; Kruger, S.J.; Frei, R.; Canfield, D.E. Atmospheric oxygenation three billion years ago. *Nature* **2013**, *501*, 535–538. [CrossRef] [PubMed]
7. Reinhard, C.T.; Planavsky, N.J.; Robbins, L.J.; Partin, C.A.; Gill, B.C.; Lalonde, S.V.; Bekker, A.; Konhauser, K.O.; Lyons, T.W. Proterozoic ocean redox and biogeochemical stasis. *Proc. Natl. Acad. Sci. USA* **2013**, *110*, 5357–5362. [CrossRef] [PubMed]
8. Canfield, D.E.; Poulton, S.W.; Knoll, A.H.; Narbonne, G.M.; Ross, G.; Goldberg, T.; Strauss, H. Ferruginous conditions dominated later neoproterozoic deep-water chemistry. *Science* **2008**, *321*, 949–952. [CrossRef] [PubMed]
9. Li, W.; Czaja, A.D.; Van Kranendonk, M.J.; Beard, B.L.; Roden, E.E.; Johnson, C.M. An anoxic, Fe(II)-rich, U-poor ocean 3.46 billion years ago. *Geochim. Cosmochim. Acta* **2013**, *120*, 65–79. [CrossRef]
10. Planavsky, N.J.; McGoldrick, P.; Scott, C.T.; Li, C.; Reinhard, C.T.; Kelly, A.E.; Chu, X.; Bekker, A.; Love, G.D.; Lyons, T.W. Widespread iron-rich conditions in the mid-Proterozoic ocean. *Nature* **2011**, *477*, 448–451. [CrossRef] [PubMed]
11. Poulton, S.W.; Canfield, D.E. Ferruginous conditions: A dominant feature of the ocean through Earth's history. *Elements* **2011**, *7*, 107–112. [CrossRef]
12. Busigny, V.; Lebeau, O.; Ader, M.; Krapež, B.; Bekker, A. Nitrogen cycle in the Late Archean ferruginous ocean. *Chem. Geol.* **2013**, *362*, 115–130. [CrossRef]
13. Farquhar, J. Atmospheric influence of Earth's earliest sulfur cycle. *Science* **2000**, *289*, 756–758. [CrossRef] [PubMed]
14. Johnson, C.M.; Beard, B.L.; Klein, C.; Beukes, N.J.; Roden, E.E. Iron isotopes constrain biologic and abiologic processes in banded iron formation genesis. *Geochim. Cosmochim. Acta* **2008**, *72*, 151–169. [CrossRef]
15. Planavsky, N.; Rouxel, O.; Bekker, A.; Shapiro, R.; Fralick, P.; Knudsen, A. Iron-oxidizing microbial ecosystems thrived in late Paleoproterozoic redox-stratified oceans. *Earth Planet. Sci. Lett.* **2009**, *286*, 230–242. [CrossRef]
16. Crowe, S.A.; Jones, C.; Katsev, S.; Magen, C.; O'Neill, A.H.; Sturm, A.; Canfield, D.E.; Haffner, G.D.; Mucci, A.; Sundby, B.; *et al*. Photoferrotrophs thrive in an Archean Ocean analogue. *Proc. Natl. Acad. Sci. USA* **2008**, *105*, 15938–15943. [CrossRef] [PubMed]

17. Walter, X.A.; Picazo, A.; Miracle, M.R.; Vicente, E.; Camacho, A.; Aragno, M.; Zopfi, J. Phototrophic Fe(II)-oxidation in the chemocline of a ferruginous meromictic lake. *Front. Microbiol.* **2014**, *5*, 713. [CrossRef] [PubMed]
18. Kappler, A.; Newman, D.K. Formation of Fe(III)-minerals by Fe(II)-oxidizing photoautotrophic bacteria. *Geochim. Cosmochim. Acta* **2004**, *68*, 1217–1226. [CrossRef]
19. Miot, J.; Benzerara, K.; Obst, M.; Kappler, A.; Hegler, F.; Schadler, S.; Bouchez, C.; Guyot, F.; Morin, G. Extracellular iron biomineralization by photoautotrophic iron-oxidizing bacteria. *Appl. Environ. Microbiol.* **2009**, *75*, 5586–5591. [CrossRef] [PubMed]
20. Cosmidis, J.; Benzerara, K.; Morin, G.; Busigny, V.; Lebeau, O.; Jézéquel, D.; Noël, V.; Dublet, G.; Othmane, G. Biomineralization of iron-phosphates in the water column of Lake Pavin (Massif Central, France). *Geochim. Cosmochim. Acta* **2014**, *126*, 78–96. [CrossRef]
21. Miot, J.; Benzerara, K.; Morin, G.; Kappler, A.; Bernard, S.; Obst, M.; Férard, C.; Skouri-Panet, F.; Guigner, J.-M.; Posth, N.; *et al*. Iron biomineralization by anaerobic neutrophilic iron-oxidizing bacteria. *Geochim. Cosmochim. Acta* **2009**, *73*, 696–711. [CrossRef]
22. Miot, J.; Benzerara, K.; Morin, G.; Bernard, S.; Beyssac, O.; Larquet, E.; Kappler, A.; Guyot, F. Transformation of vivianite by anaerobic nitrate-reducing iron-oxidizing bacteria. *Geobiology* **2009**, *7*, 373–384. [CrossRef] [PubMed]
23. Miot, J.; Li, J.; Benzerara, K.; Sougrati, M.T.; Ona-Nguema, G.; Bernard, S.; Jumas, J.-C.; Guyot, F. Formation of single domain magnetite by green rust oxidation promoted by microbial anaerobic nitrate-dependent iron oxidation. *Geochim. Cosmochim. Acta* **2014**, *139*, 327–343. [CrossRef]
24. Lehours, A.-C.; Batisson, I.; Guedon, A.; Mailhot, G.; Fonty, G. Diversity of culturable bacteria, from the Anaerobic Zone of the meromictic Lake Pavin, able to perform dissimilatory-iron reduction in different *in vitro* conditions. *Geomicrobiol. J.* **2009**, *26*, 212–223. [CrossRef]
25. Fredrickson, J.K.; Zachara, J.M.; Kennedy, D.W.; Dong, H.; Onstott, T.C.; Hinman, N.W.; Li, S. Biogenic iron mineralization accompanying the dissimilatory reduction of hydrous ferric oxide by a groundwater bacterium. *Geochim. Cosmochim. Acta* **1998**, *62*, 3239–3257. [CrossRef]
26. Kukkadapu, R.K.; Zachara, J.M.; Fredrickson, J.K.; Kennedy, D.W. Biotransformation of two-line silica-ferrihydrite by a dissimilatory Fe(III)-reducing bacterium: Formation of carbonate green rust in the presence of phosphate. *Geochim. Cosmochim. Acta* **2004**, *68*, 2799–2814. [CrossRef]
27. Ona-Nguema, G.; Abdelmoula, M.; Jorand, F.; Benali, O.; Block, J.-C.; Génin, J.-M.R. Iron(II,III) hydroxycarbonate green rust formation and stabilization from lepidocrocite bioreduction. *Environ. Sci. Technol.* **2002**, *36*, 16–20. [CrossRef] [PubMed]
28. Zegeye, A.; Bonneville, S.; Benning, L.G.; Sturm, A.; Fowle, D.A.; Jones, C.; Canfield, D.E.; Ruby, C.; MacLean, L.C.; Nomosatryo, S.; *et al*. Green rust formation controls nutrient availability in a ferruginous water column. *Geology* **2012**, *40*, 599–602. [CrossRef]
29. Zegeye, A.; Mustin, C.; Jorand, F. Bacterial and iron oxide aggregates mediate secondary iron mineral formation: Green rust *versus* magnetite: Iron oxide aggregation and green rust formation. *Geobiology* **2010**, *8*, 209–222. [CrossRef] [PubMed]
30. Etique, M.; Jorand, F.P.A.; Zegeye, A.; Grégoire, B.; Despas, C.; Ruby, C. Abiotic process for Fe(II) oxidation and green rust mineralization driven by a heterotrophic nitrate reducing bacteria (*Klebsiella mobilis*). *Environ. Sci. Technol.* **2014**, *48*, 3742–3751. [CrossRef] [PubMed]
31. Pantke, C.; Obst, M.; Benzerara, K.; Morin, G.; Ona-Nguema, G.; Dippon, U.; Kappler, A. Green rust formation during Fe(II) oxidation by the nitrate-reducing *Acidovorax* sp. strain BoFeN1. *Environ. Sci. Technol.* **2012**, *46*, 1439–1446. [CrossRef] [PubMed]
32. Biderre-Petit, C.; Boucher, D.; Kuever, J.; Alberic, P.; Jézéquel, D.; Chebance, B.; Borrel, G.; Fonty, G.; Peyret, P. Identification of sulfur-cycle prokaryotes in a low-sulfate lake (Lake Pavin) using aprA and 16S rRNA gene markers. *Microb. Ecol.* **2011**, *61*, 313–327. [CrossRef] [PubMed]
33. Bura-Nakić, E.; Viollier, E.; Ciglenečki, I. Electrochemical and colorimetric measurements show the dominant role of FeS in a permanently anoxic lake. *Environ. Sci. Technol.* **2013**, *47*, 741–749. [CrossRef] [PubMed]
34. Bura-Nakić, E.; Viollier, E.; Jézéquel, D.; Thiam, A.; Ciglenečki, I. Reduced sulfur and iron species in anoxic water column of meromictic crater Lake Pavin (Massif Central, France). *Chem. Geol.* **2009**, *266*, 311–317. [CrossRef]
35. Donald, R.; Southam, G. Low temperature anaerobic bacterial diagenesis of ferrous monosulfide to pyrite. *Geochim. Cosmochim. Acta* **1999**, *63*, 2019–2023. [CrossRef]

36. Chan, C.S.; Fakra, S.C.; Emerson, D.; Fleming, E.J.; Edwards, K.J. Lithotrophic iron-oxidizing bacteria produce organic stalks to control mineral growth: Implications for biosignature formation. *ISME J.* **2011**, *5*, 717–727. [CrossRef] [PubMed]
37. Labrenz, M.; Banfield, J.F. Sulfate-reducing bacteria-dominated biofilms that precipitate ZnS in a subsurface circumneutral-pH mine drainage system. *Microb. Ecol.* **2004**, *47*, 205–217. [CrossRef] [PubMed]
38. Bazylinski, D.A.; Frankel, R.B.; Konhauser, K.O. Modes of biomineralization of magnetite by microbes. *Geomicrobiol. J.* **2007**, *24*, 465–475. [CrossRef]
39. Benzerara, K.; Skouri-Panet, F.; Li, J.; Férard, C.; Gugger, M.; Laurent, T.; Couradeau, E.; Ragon, M.; Cosmidis, J.; Menguy, N.; *et al*. Intracellular Ca-carbonate biomineralization is widespread in cyanobacteria. *Proc. Natl. Acad. Sci. USA* **2014**, *111*, 10933–10938. [CrossRef] [PubMed]
40. Couradeau, E.; Benzerara, K.; Gerard, E.; Moreira, D.; Bernard, S.; Brown, G.E.; Lopez-Garcia, P. An early-branching microbialite cyanobacterium forms intracellular carbonates. *Science* **2012**, *336*, 459–462. [CrossRef] [PubMed]
41. Lefevre, C.T.; Menguy, N.; Abreu, F.; Lins, U.; Posfai, M.; Prozorov, T.; Pignol, D.; Frankel, R.B.; Bazylinski, D.A. A cultured greigite-producing magnetotactic bacterium in a novel group of sulfate-reducing bacteria. *Science* **2011**, *334*, 1720–1723. [CrossRef] [PubMed]
42. Melton, E.D.; Stief, P.; Behrens, S.; Kappler, A.; Schmidt, C. High spatial resolution of distribution and interconnections between Fe- and N-redox processes in profundal lake sediments: Microbial Fe and N redox cycling in lake sediments. *Environ. Microbiol.* **2014**, *16*, 3287–3303. [CrossRef] [PubMed]
43. Kjeldsen, K.U.; Loy, A.; Jakobsen, T.F.; Thomsen, T.R.; Wagner, M.; Ingvorsen, K. Diversity of sulfate-reducing bacteria from an extreme hypersaline sediment, Great Salt Lake (Utah): Diversity of SRB in Great Salt Lake. *FEMS Microbiol. Ecol.* **2007**, *60*, 287–298. [CrossRef] [PubMed]
44. Rees, G.N.; Baldwin, D.S.; Watson, G.O.; Hall, K.C. Sulfide formation in freshwater sediments, by sulfate-reducing microorganisms with diverse tolerance to salt. *Sci. Total Environ.* **2010**, *409*, 134–139. [CrossRef] [PubMed]
45. Michard, G.; Viollier, E.; Jézéquel, D.; Sarazin, G. Geochemical study of a crater lake: Pavin Lake, France—Identification, location and quantification of the chemical reactions in the lake. *Chem. Geol.* **1994**, *115*, 103–115. [CrossRef]
46. Viollier, E.; Michard, G.; Jézéquel, D.; Pèpe, M.; Sarazin, G. Geochemical study of a crater lake: Lake Pavin, Puy de Dôme, France. Constraints afforded by the particulate matter distribution in the element cycling within the lake. *Chem. Geol.* **1997**, *142*, 225–241. [CrossRef]
47. Podda, F.; Michard, G. Mesure colorimétrique de l'alcalinité. *C. R. Acad. Sci.* **1994**, *319*, 651–657. (In French)
48. Lehours, A.-C.; Bardot, C.; Thenot, A.; Debroas, D.; Fonty, G. Anaerobic microbial communities in Lake Pavin, a unique meromictic lake in France. *Appl. Environ. Microbiol.* **2005**, *71*, 7389–7400. [CrossRef] [PubMed]
49. Viollier, E.; Jézéquel, D.; Michard, G.; Pèpe, M.; Sarazin, G.; Alberic, P. Geochemical study of a crater lake (Pavin Lake, France): Trace-element behaviour in the monimolimnion. *Chem. Geol.* **1995**, *125*, 61–72. [CrossRef]
50. Grami, B.; Rasconi, S.; Niquil, N.; Jobard, M.; Saint-Béat, B.; Sime-Ngando, T. Functional effects of parasites on food web properties during the spring diatom bloom in Lake Pavin: A linear inverse modeling analysis. *PLoS ONE* **2011**, *6*, e23273. [CrossRef] [PubMed]
51. Rasconi, S.; Grami, B.; Niquil, N.; Jobard, M.; Sime-Ngando, T. Parasitic chytrids sustain zooplankton growth during inedible algal bloom. *Front. Microbiol.* **2014**, *5*, 229. [CrossRef] [PubMed]
52. Ragon, M.; Benzerara, K.; Moreira, D.; Tavera, R.; López-García, P. 16S rDNA-based analysis reveals cosmopolitan occurrence but limited diversity of two cyanobacterial lineages with contrasted patterns of intracellular carbonate mineralization. *Front. Microbiol.* **2014**, *5*. [CrossRef] [PubMed]
53. Tebo, B.M.; Johnson, H.A.; McCarthy, J.K.; Templeton, A.S. Geomicrobiology of manganese(II) oxidation. *Trends Microbiol.* **2005**, *13*, 421–428. [CrossRef] [PubMed]
54. Geszvain, K.; McCarthy, J.K.; Tebo, B.M. Elimination of manganese(II,III) oxidation in pseudomonas putida GB-1 by a double knockout of two putative multicopper oxidase genes. *Appl. Environ. Microbiol.* **2013**, *79*, 357–366. [CrossRef] [PubMed]
55. Geszvain, K.; Butterfield, C.; Davis, R.E.; Madison, A.S.; Lee, S.; Parker, D.L.; Soldatova, A.; Spiro, T.G.; Luther, G.W.; Tebo, B.M. The molecular biogeochemistry of manganese(II) oxidation. *Biochem. Soc. Trans.* **2012**, *40*, 1244–1248. [CrossRef] [PubMed]
56. Learman, D.R.; Voelker, B.M.; Vazquez-Rodriguez, A.I.; Hansel, C.M. Formation of manganese oxides by bacterially generated superoxide. *Nat. Geosci.* **2011**, *4*, 95–98. [CrossRef]

57. Keim, C.N.; Nalini, H.A.; de Lena, J.C. Manganese oxide biominerals from freshwater environments in Quadrilatero Ferrifero, Minas Gerais, Brazil. *Geomicrobiol. J.* **2015**, *32*, 549–559. [CrossRef]
58. Chubar, N.; Avramut, C.; Visser, T. Formation of manganese phosphate and manganese carbonate during long-term sorption of Mn^{2+} by viable Shewanella putrefaciens: Effects of contact time and temperature. *Environ. Sci. Process. Impacts* **2015**, *17*, 780–790. [CrossRef] [PubMed]
59. Friedl, G.; Wehrli, B.; Manceau, A. Solid phases in the cycling of manganese in eutrophic lakes: New insights from EXAFS spectroscopy. *Geochim. Cosmochim. Acta* **1997**, *61*, 275–290. [CrossRef]
60. Jones, C.; Crowe, S.A.; Sturm, A.; Leslie, K.L.; MacLean, L.C.W.; Katsev, S.; Henny, C.; Fowle, D.A.; Canfield, D.E. Biogeochemistry of manganese in ferruginous Lake Matano, Indonesia. *Biogeosciences* **2011**, *8*, 2977–2991. [CrossRef]
61. Carrias, J.-F.; Thouvenot, A.; Amblard, C.; Sime-Ngando, T. Dynamics and growth estimates of planktonic protists during early spring in Lake Pavin, France. *Aquat. Microb. Ecol.* **2001**, *24*, 163–174. [CrossRef]
62. Dupraz, C.; Reid, R.P.; Braissant, O.; Decho, A.W.; Norman, R.S.; Visscher, P.T. Processes of carbonate precipitation in modern microbial mats. *Earth Sci. Rev.* **2009**, *96*, 141–162. [CrossRef]
63. Buffle, J.; De Vitre, R.R.; Perret, D.; Leppard, G.G. Physico-chemical characteristics of a colloidal iron phosphate species formed at the oxic-anoxic interface of a eutrophic lake. *Geochim. Cosmochim. Acta* **1989**, *53*, 399–408. [CrossRef]
64. Lienemann, C.P.; Monnerat, M.; Dominik, J.; Perret, D. Identification of stoichiometric iron-phosphorus colloids produced in a eutrophic lake. *Aquat. Sci.* **1999**, *61*, 133–149. [CrossRef]
65. Voegelin, A.; Senn, A.-C.; Kaegi, R.; Hug, S.J.; Mangold, S. Dynamic Fe-precipitate formation induced by Fe(II) oxidation in aerated phosphate-containing water. *Geochim. Cosmochim. Acta* **2013**, *117*, 216–231. [CrossRef]
66. Senn, A.-C.; Kaegi, R.; Hug, S.J.; Hering, J.G.; Mangold, S.; Voegelin, A. Composition and structure of Fe(III)-precipitates formed by Fe(II) oxidation in water at near-neutral pH: Interdependent effects of phosphate, silicate and Ca. *Geochim. Cosmochim. Acta* **2015**, *162*, 220–246. [CrossRef]
67. Lefèvre, C.T. Genomic insights into the early-diverging magnetotactic bacteria. *Environ. Microbiol.* **2016**, *18*, 1–3. [CrossRef] [PubMed]
68. Lefevre, C.T.; Bazylinski, D.A. Ecology, diversity, and evolution of magnetotactic bacteria. *Microbiol. Mol. Biol. Rev.* **2013**, *77*, 497–526. [CrossRef] [PubMed]
69. Lehours, A.-C.; Evans, P.; Bardot, C.; Joblin, K.; Gerard, F. Phylogenetic diversity of archaea and bacteria in the anoxic zone of a meromictic lake (Lake Pavin, France). *Appl. Environ. Microbiol.* **2007**, *73*, 2016–2019. [CrossRef] [PubMed]
70. Emerson, D.; Fleming, E.J.; McBeth, J.M. Iron-oxidizing bacteria: An environmental and genomic perspective. *Annu. Rev. Microbiol.* **2010**, *64*, 561–583. [CrossRef] [PubMed]
71. Emerson, D.; Merrill Floyd, M. Enrichment and isolation of iron-oxidizing bacteria at neutral pH. In *Methods in Enzymology*; Elsevier: Amsterdam, The Netherlands, 2005; Volume 397, pp. 112–123.
72. Chan, C.S. Microbial polysaccharides template assembly of nanocrystal fibers. *Science* **2004**, *303*, 1656–1658. [CrossRef] [PubMed]
73. Comolli, L.R.; Luef, B.; Chan, C.S. High-resolution 2D and 3D cryo-TEM reveals structural adaptations of two stalk-forming bacteria to an Fe-oxidizing lifestyle: 3D cryo-TEM of Fe-oxidizing bacteria. *Environ. Microbiol.* **2011**, *13*, 2915–2929. [CrossRef] [PubMed]
74. Fleming, E.J.; Langdon, A.E.; Martinez-Garcia, M.; Stepanauskas, R.; Poulton, N.J.; Masland, E.D.P.; Emerson, D. What's new is old: Resolving the identity of *Leptothrix ochracea* using single cell genomics, pyrosequencing and FISH. *PLoS ONE* **2011**, *6*, e17769. [CrossRef] [PubMed]
75. Seder-Colomina, M.; Morin, G.; Benzerara, K.; Ona-Nguema, G.; Pernelle, J.-J.; Esposito, G.; Van Hullebusch, E.D. *Sphaerotilus natans*, a neutrophilic iron-related sheath-forming bacterium: Perspectives for metal remediation strategies. *Geomicrobiol. J.* **2014**, *31*, 64–75. [CrossRef]
76. Banfield, J.F. Aggregation-based crystal growth and microstructure development in natural iron oxyhydroxide biomineralization products. *Science* **2000**, *289*, 751–754. [CrossRef] [PubMed]
77. Melton, E.D.; Schmidt, C.; Kappler, A. Microbial iron(II) oxidation in littoral freshwater lake sediment: The tpotential for competition between phototrophic *vs.* nitrate-reducing iron(II)-oxidizers. *Front. Microbiol.* **2012**, *3*, 197. [CrossRef] [PubMed]
78. Reguera, G.; Nevin, K.P.; Nicoll, J.S.; Covalla, S.F.; Woodard, T.L.; Lovley, D.R. Biofilm and nanowire production leads to increased current in geobacter sulfurreducens fuel cells. *Appl. Environ. Microbiol.* **2006**, *72*, 7345–7348. [CrossRef] [PubMed]

79. Lehours, A.-C.; Rabiet, M.; Morel-Desrosiers, N.; Morel, J.-P.; Jouve, L.; Arbeille, B.; Mailhot, G.; Fonty, G. Ferric iron reduction by fermentative strain BS2 isolated from an iron-rich anoxic environment (Lake Pavin, France). *Geomicrobiol. J.* **2010**, *27*, 714–722. [CrossRef]
80. Dohnalkova, A.C.; Marshall, M.J.; Arey, B.W.; Williams, K.H.; Buck, E.C.; Fredrickson, J.K. Imaging hydrated microbial extracellular polymers: Comparative analysis by electron microscopy. *Appl. Environ. Microbiol.* **2011**, *77*, 1254–1262. [CrossRef] [PubMed]
81. Miot, J.; Benzerara, K.; Kappler, A. Investigating microbe-mineral interactions: Recent advances in X-ray and electron microscopy and redox-sensitive methods. *Annu. Rev. Earth Planet. Sci.* **2014**, *42*, 271–289. [CrossRef]
82. Maki, J.S. Bacterial intracellular sulfur globules: Structure and function. *J. Mol. Microbiol. Biotechnol.* **2013**, *23*, 270–280. [CrossRef] [PubMed]
83. Devaux, J. Contribution a l'etude limnologique du Lac Pavin (France) I: Facteurs abiotiques et phytoplancton. *Hydrobiologia* **1980**, *68*, 167–189. (In French). [CrossRef]
84. Ghosh, W.; Dam, B. Biochemistry and molecular biology of lithotrophic sulfur oxidation by taxonomically and ecologically diverse bacteria and archaea. *FEMS Microbiol. Rev.* **2009**, *33*, 999–1043. [CrossRef] [PubMed]
85. De Gusseme, B.; De Schryver, P.; De Cooman, M.; Verbeken, K.; Boeckx, P.; Verstraete, W.; Boon, N. Nitrate-reducing, sulfide-oxidizing bacteria as microbial oxidants for rapid biological sulfide removal: NR-SOB as microbial oxidants for biological sulfide removal. *FEMS Microbiol. Ecol.* **2009**, *67*, 151–161. [CrossRef] [PubMed]
86. Campbell, B.J.; Engel, A.S.; Porter, M.L.; Takai, K. The versatile ε-proteobacteria: Key players in sulphidic habitats. *Nat. Rev. Microbiol.* **2006**, *4*, 458–468. [CrossRef] [PubMed]
87. Vetriani, C.; Tran, H.V.; Kerkhof, L.J. Fingerprinting microbial assemblages from the oxic/anoxic chemocline of the Black Sea. *Appl. Environ. Microbiol.* **2003**, *69*, 6481–6488. [CrossRef] [PubMed]
88. Bonny, S.M.; Jones, B. Experimental precipitation of barite ($BaSO_4$) among streamers of sulfur-oxidizing bacteria. *J. Sediment. Res.* **2008**, *78*, 357–365. [CrossRef]
89. Bonny, S.M.; Jones, B. Barite ($BaSO_4$) biomineralization at Flybye Springs, a cold sulphur spring system in Canada's Northwest Territories. *Can. J. Earth Sci.* **2007**, *44*, 835–856. [CrossRef]
90. Senko, J.M.; Campbell, B.S.; Henriksen, J.R.; Elshahed, M.S.; Dewers, T.A.; Krumholz, L.R. Barite deposition resulting from phototrophic sulfide-oxidizing bacterial activity. *Geochim. Cosmochim. Acta* **2004**, *68*, 773–780. [CrossRef]
91. Karnachuk, S.; Kurochkina, O.; Tuovin, O. Growth of sulfate-reducing bacteria with solid-phase electron acceptors. *Appl. Microbiol. Biotechnol.* **2002**, *58*, 482–486. [CrossRef] [PubMed]
92. Francois, F.; Lombard, C.; Guigner, J.-M.; Soreau, P.; Brian-Jaisson, F.; Martino, G.; Vandervennet, M.; Garcia, D.; Molinier, A.-L.; Pignol, D.; *et al*. Isolation and characterization of environmental bacteria capable of extracellular biosorption of mercury. *Appl. Environ. Microbiol.* **2012**, *78*, 1097–1106. [CrossRef] [PubMed]
93. Hellal, J.; Guédron, S.; Huguet, L.; Schäfer, J.; Laperche, V.; Joulian, C.; Lanceleur, L.; Burnol, A.; Ghestem, J.-P.; Garrido, F.; *et al*. Mercury mobilization and speciation linked to bacterial iron oxide and sulfate reduction: A column study to mimic reactive transfer in an anoxic aquifer. *J. Contam. Hydrol.* **2015**, *180*, 56–68. [CrossRef] [PubMed]
94. Zhang, T.; Kucharzyk, K.H.; Kim, B.; Deshusses, M.A.; Hsu-Kim, H. Net methylation of mercury in estuarine sediment microcosms amended with dissolved, nanoparticulate, and microparticulate mercuric sulfides. *Environ. Sci. Technol.* **2014**, *48*, 9133–9141. [CrossRef] [PubMed]
95. Zhang, T.; Kim, B.; Levard, C.; Reinsch, B.C.; Lowry, G.V.; Deshusses, M.A.; Hsu-Kim, H. Methylation of mercury by bacteria exposed to dissolved, nanoparticulate, and microparticulate mercuric sulfides. *Environ. Sci. Technol.* **2012**, *46*, 6950–6958. [CrossRef] [PubMed]
96. Pham, A.L.-T.; Morris, A.; Zhang, T.; Ticknor, J.; Levard, C.; Hsu-Kim, H. Precipitation of nanoscale mercuric sulfides in the presence of natural organic matter: Structural properties, aggregation, and biotransformation. *Geochim. Cosmochim. Acta* **2014**, *133*, 204–215. [CrossRef]
97. Li, J.; Benzerara, K.; Bernard, S.; Beyssac, O. The link between biomineralization and fossilization of bacteria: Insights from field and experimental studies. *Chem. Geol.* **2013**, *359*, 49–69. [CrossRef]